ICES REPORT 10-46

November 2010

Isogeometric Analysis-Based Goal-Oriented Error Estimation for Free-Boundary Problems

by

K.G. van der Zee and C.V. Verhoosel

The Institute for Computational Engineering and Sciences
The University of Texas at Austin
Austin, Texas 78712

*Reference: K.G. van der Zee and C.V. Verhoosel, "**Isogeometric Analysis-Based Goal-Oriented Error Estimation for Free-Boundary Problems**", ICES REPORT 10-46, The Institute for Computational Engineering and Sciences, The University of Texas at Austin, November 2010.*

Isogeometric Analysis-Based Goal-Oriented Error Estimation for Free-Boundary Problems

K.G. van der Zee[*,a], C.V. Verhoosel[b]

[a] *Institute for Computational Engineering and Sciences (ICES), The University of Texas at Austin, 201 East 24th Street, 1 University Station C0200, Austin, TX 78712, USA*

[b] *Department of Mechanical Engineering, Eindhoven University of Technology, P.O. Box 513, 5600 MB Eindhoven, The Netherlands*

Abstract

We consider goal-oriented error estimation for free-boundary problems using isogeometric analysis. Goal-oriented methods require the solution of the dual problem, which is a problem for the adjoint of the linearized free-boundary problem. Owing to linearization, this dual problem includes a curvature-dependent boundary condition, which leads to cumbersome implementations if the discrete free-boundary is only continuous, as in a piecewise-linear representation. Isogeometric finite elements straightforwardly provide continuously differentiable free boundaries for which the corresponding dual problem can be easily implemented.

We illustrate the computation of the linearized-adjoint problems with two test cases and estimate the error in corresponding quantities of interest. In the first problem, a single B-spline patch can be employed. In the second problem, we employ T-splines. Bézier extraction is used to provide a finite element interface to these two distinct spline technologies.

Key words: isogeometric analysis, goal-oriented analysis, Bernoulli free boundary problem, B-splines, non-uniform rational B-splines (NURBS), T-splines, Bézier extraction, a posteriori error estimation, shape-linearized adjoint, duality

[*] Corresponding author

Email addresses: vanderzee@ices.utexas.edu (K.G. van der Zee), c.v.verhoosel@tue.nl (C.V. Verhoosel)

1. Introduction

Motivated by the synthesis of computer aided geometric design (CAGD) and finite element analysis (FEA), *isogeometric analysis* (IGA) has arisen, which employs the same smooth functions used for geometry (non-uniform rational B-splines (NURBS), T-splines, etc.) as basis functions for analysis [9, 22]. The relative ease with which such basis functions can be generated with arbitrary smoothness, i.e., up to C^{p-1}-continuity for pth-order splines, has generated an offspring of numerical applications where higher-order continuity is advantageous; see e.g. [2, 5, 8–10, 19, 37]. The current work shows that higher-order continuity is also advantageous in the simulation of free-boundary problems.

A free-boundary problem is a problem which requires the simultaneous solution of both the unknown function and its domain of definition (through the position of the free boundary). Free-boundary problems arise in various applications such as free-surface flow, fluid–structure interaction and solidification. The fact that the geometry of the underlying domain is an unknown, makes these problems inherently nonlinear. Moreover, the linearization of these geometrical nonlinearities is far from trivial. Typically, the linearization of free-boundary problems leads to *curvature*-dependent terms [7, 18, 23, 24]. Of course, such terms only make sense if the curvature is bounded, i.e., if the boundary is sufficiently smooth (e.g. C^1). For example, in a finite-element simulation, if a discrete free-boundary has a piecewise-linear representation, then the curvature is singular (infinite, of Dirac delta-type) at the element intersections (where there is a kink in the geometry). It is exactly for this reason that *linearization at smooth geometries is preferred*.

An important application of linearization are linearized-adjoints as employed in the field of *goal-oriented analysis* [3, 28]. In goal-oriented error estimation, an estimate of the error in specific quantities of interests is computed, employing the solution to a (linearized-) adjoint problem, the so-called *dual* problem. The development of goal-oriented error estimates and their adaptive strategies go back to the late 1990s, and as such has extended the theory of a posteriori error estimates in global norms [1]. Let us remark that another important application of linearization are Newton-based solution algorithms. We shall not consider that application in this work.

An approach to the linearized-adjoint of a model free-boundary problem, the so-called Bernoulli free-boundary problem, has recently been presented in [36] (in the context of goal-oriented error estimation). To perform the linearization, this approach uses shape derivatives [13, 32] as familiar in shape optimization [27].

The resulting dual problem corresponds to a Laplace problem with a curvature-dependent Robin boundary condition. Since in [36] the discrete free boundaries were piecewise linear, the curvature term in the dual problem led to a cumbersome implementation.

In the current work, we reconsider the goal-oriented error estimation of the Bernoulli free-boundary problem, but now using C^1 isogeometric finite elements. Since the discrete free-boundaries are C^1-continuous, the curvature is bounded, and the dual problem can easily be implemented, as is. Following an introduction of the Bernoulli free-boundary problem and its discretization in Section 2, we briefly recall from [36] the derivation of the linearized-adjoint and the goal-oriented error estimate in Section 3. We present details of the B-spline and T-spline shape functions, as well as their implementation using Bézier extraction in Section 4. Numerical simulations are discussed in Section 5.

2. The Bernoulli free-boundary problem

We consider the (steady) Bernoulli free-boundary problem in $\mathbb{R}^2$. This problem seeks an a priori unknown domain $\Omega \subset \mathbb{R}^2$, for which the boundary $\partial\Omega$ consists of a free part Γ and fixed part $\Gamma_{\mathcal{D}}$, and a corresponding function $u : \Omega \to \mathbb{R}$ such that

$$-\Delta u = f \qquad \text{in } \Omega\,, \tag{1a}$$

$$\frac{\partial u}{\partial n} = g \qquad \text{on } \Gamma\,, \tag{1b}$$

$$u = u_{\mathcal{D}} = 1 \qquad \text{on } \Gamma\,, \tag{1c}$$

$$u = u_{\mathcal{D}} \qquad \text{on } \Gamma_{\mathcal{D}}\,, \tag{1d}$$

where $\partial(\cdot)/\partial n \equiv \boldsymbol{n} \cdot \nabla(\cdot)$, with $\boldsymbol{n}$ being the unit outward normal. We assume that the functions f, g and $u_{\mathcal{D}}$ defining the data are sufficiently smooth. Furthermore, we assume that $u_{\mathcal{D}} \neq 1$ on some part of $\Gamma_{\mathcal{D}}$, and $g \geq g_0 > 0$ with g_0 a constant.

The problem described by (1) is a classical model for free-boundary problems such as encountered in free surface flow and Stefan problems. In a free surface flow interpretation of (1), Γ represents the free surface and u can represent the stream function for a steady free-surface potential flow [23]. An overview of analysis and algorithms for (1) can be found in Flucher and Rumpf [18].

2.1. Domain and free-boundary parameterization

To deal with variable domains, it is convenient to introduce parameterizations based on the free-boundary displacement. Let Ω_0 denote a reference domain and

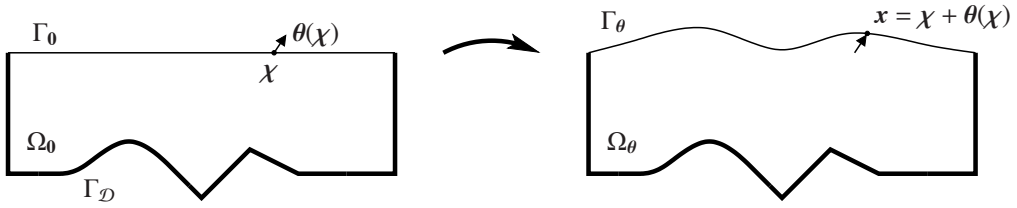

Figure 1: Illustration of the parameterization of the free boundary Γ_θ by its displacement $\boldsymbol{\theta}$ with respect to the reference configuration Γ_0.

Γ_0 the reference free boundary. We then denote the free-boundary displacement by $\boldsymbol{\theta}$, which is a vectorfield defined on Γ_0. The current free boundary Γ_θ is then given by

$$\Gamma_\theta = \left\{ \boldsymbol{x} = \boldsymbol{\chi} + \boldsymbol{\theta}(\boldsymbol{\chi}) \,,\ \forall \boldsymbol{\chi} \in \Gamma_0 \right\} .$$

We denote the corresponding domain by Ω_θ. A graphical illustration of this parameterization is depicted in Fig. 1.

An important advantage of introducing this parameterization is that we can now formulate our problem (1) in terms of the pair $(u, \boldsymbol{\theta})$.

2.2. Weak formulation

To introduce a weak formulation of (1), for each $\boldsymbol{\theta}$, we define V_θ to be the space of test functions in the Sobolev space $H^1(\Omega_\theta)$ which are zero *on* $\Gamma_{\mathcal{D}}$ *only*, i.e.,

$$V_\theta \equiv V(\Omega_\theta) \overset{\text{def}}{=} \left\{ v \in H^1(\Omega_\theta) \,\middle|\, v = 0 \text{ on } \Gamma_{\mathcal{D}} \right\} .$$

Similarly, we define W_θ to be the (affine) space of trial functions in $H^1(\Omega_\theta)$ which are equal to $u_{\mathcal{D}}$ *on the whole boundary* $\partial\Omega_\theta$, i.e.,

$$W_\theta \equiv W(\Omega_\theta) \overset{\text{def}}{=} \left\{ w \in H^1(\Omega_\theta) \,\middle|\, w = u_{\mathcal{D}} \text{ on } \partial\Omega_\theta \right\} .$$

We denote the space for suitable displacements $\boldsymbol{\theta}$ by $\boldsymbol{\Theta}$.[1] Next, we multiply (1a) by a test function v, integrate over Ω_θ, integrate by parts, and substitute the Neumann

[1] The space $\boldsymbol{\Theta}$ typically consists of Lipschitz-continuous (vector-valued) functions defined on Γ_0 which are zero on the endpoints of Γ_0; cf. [35].

boundary condition. We then arrive at the following weak formulation:

$$\left.\begin{aligned} &\text{Find } (\boldsymbol{\theta}, u) \in \boldsymbol{\Theta} \times W_{\boldsymbol{\theta}} \text{ such that:} \\ &\quad \mathcal{B}((\boldsymbol{\theta}, u); v) = \mathcal{L}(\boldsymbol{\theta}; v) \qquad \forall v \in V_{\boldsymbol{\theta}} \ , \end{aligned}\right\} \tag{2}$$

where

$$\mathcal{B}((\boldsymbol{\theta}, u); v) \overset{\text{def}}{=} \int_{\Omega_{\boldsymbol{\theta}}} \nabla u \cdot \nabla v \, \mathrm{d}x \ , \tag{3a}$$

$$\mathcal{L}(\boldsymbol{\theta}; v) \overset{\text{def}}{=} \int_{\Omega_{\boldsymbol{\theta}}} f \, v \, \mathrm{d}x + \int_{\Gamma_{\boldsymbol{\theta}}} g \, v \, \mathrm{d}s \ . \tag{3b}$$

Remark 2.1 (Geometric nonlinearity) The dependence of $\mathcal{B}$ and $\mathcal{L}$ on $\boldsymbol{\theta}$ is of geometric nature, essentially defining the domains of integration. Furthermore, the same dependence appears in the spaces $V_{\boldsymbol{\theta}}$ and $W_{\boldsymbol{\theta}}$. These nonstandard geometric dependencies lead to a nontrivial linearization in Section 3. □

2.3. Moving-mesh Galerkin discretization

To discretize the weak formulation (2), we consider a moving-mesh approach (corresponds to ALE methods in dynamic settings [14]). As usual in a Galerkin procedure, we shall replace the infinite-dimensional spaces $V_{\boldsymbol{\theta}}$, $W_{\boldsymbol{\theta}}$ and $\boldsymbol{\Theta}$ in (2) by suitable discrete finite-element spaces. To define these spaces we first introduce a partition $\mathcal{P}^h_{\mathbf{0}}$ (the reference mesh) of the reference domain $\Omega_{\mathbf{0}}$ into nonoverlapping elements $K_{\mathbf{0}}$ (of diameter $\leq h$). The space of basis functions $\bar{N}_i$, $i = 1, \ldots, n$, defined with respect to the mesh $\mathcal{P}^h_{\mathbf{0}}$ is denoted

$$S^h \overset{\text{def}}{=} \operatorname{Span}\left\{\bar{N}_i \, , \, i = 1, \ldots, n\right\} .$$

We discuss the basis functions used in isogeometric analysis in Section 4. We can then introduce the discrete test and trial space on the reference domain as:

$$V^h_{\mathbf{0}} \overset{\text{def}}{=} S^h \cap V_{\mathbf{0}} \ ,$$
$$W^h_{\mathbf{0}} \overset{\text{def}}{=} S^h \cap W_{\mathbf{0}} \ ,$$

respectively. Note that the functions in $V^h_{\mathbf{0}}$ are zero on $\Gamma_{\mathcal{D}}$ and those in $W_{\mathbf{0}}$ equal $u_{\mathcal{D}}$ on $\partial\Omega_{\mathbf{0}}$.

Following the isoparametric/isogeometric concept [9, 21], we obtain approximate deformed domains Ω^h by constructing discrete geometry maps $\mathbf{T}^h : \Omega_\mathbf{0} \to \Omega^h$ using the functions in $V_\mathbf{0}^h$ as follows:

$$\boldsymbol{x} = \mathbf{T}^h(\boldsymbol{\chi}) = \sum_{i=1}^{n} \bar{N}_i(\boldsymbol{\chi})\, \boldsymbol{X}_i \,, \qquad \forall \boldsymbol{\chi} \in \Omega_\mathbf{0} \,, \tag{4}$$

where $\boldsymbol{X}_i$ are suitable points (control points in isogeometric analysis, see Sec. 4). A discrete map $\mathbf{T}^h$ induces a particular discrete free-boundary displacement $\boldsymbol{\theta}^h$ and corresponding discrete free boundary $\Gamma_{\boldsymbol{\theta}^h}$:

$$\begin{aligned} \boldsymbol{\theta}^h(\boldsymbol{\chi}) &= \mathbf{T}^h(\boldsymbol{\chi}) - \boldsymbol{\chi} \,, \qquad \forall \boldsymbol{\chi} \in \Gamma_\mathbf{0} \,, \\ \Gamma_{\boldsymbol{\theta}^h} &= \left\{ \boldsymbol{x} = \boldsymbol{\chi} + \boldsymbol{\theta}^h(\boldsymbol{\chi}) \,,\ \forall \boldsymbol{\chi} \in \Gamma_\mathbf{0} \right\} . \end{aligned}$$

We collect all such discrete free-boundary displacements in the discrete space $\boldsymbol{\Theta}^h$.

Clearly, to a certain free-boundary displacement $\boldsymbol{\theta}^h$, there correspond multiple maps $\mathbf{T}^h$, i.e. $\mathbf{T}^h$ is not uniquely determined inside $\Omega_\mathbf{0}$. To determine $\mathbf{T}^h$ uniquely, we solve a discrete fictitious linear elasticity problem with given boundary displacements [5, 14, 16], and denote that unique map by

$$\mathbf{T}_{\boldsymbol{\theta}^h} : \Omega_\mathbf{0} \to \Omega_{\boldsymbol{\theta}^h} \,.$$

We can now introduce the mesh $\mathcal{P}^h_{\boldsymbol{\theta}^h}$ in the domain $\Omega_{\boldsymbol{\theta}}$:

$$\mathcal{P}^h_{\boldsymbol{\theta}^h} \overset{\text{def}}{=} \left\{ K = \mathbf{T}_{\boldsymbol{\theta}^h}(K_\mathbf{0}) \,,\ \forall K_\mathbf{0} \in \mathcal{P}^h_\mathbf{0} \right\} .$$

An example of a reference mesh and corresponding current mesh is illustrated in Fig. 8 (bottom row) in Section 5. The discrete spaces in the domain $\Omega_{\boldsymbol{\theta}}$ are:

$$\begin{aligned} V^h_{\boldsymbol{\theta}^h} &\overset{\text{def}}{=} \left\{ v = \bar{v} \circ \mathbf{T}_{\boldsymbol{\theta}^h} \,,\ \forall \bar{v} \in V^h_\mathbf{0} \right\} , \\ W^h_{\boldsymbol{\theta}^h} &\overset{\text{def}}{=} \left\{ w = \bar{w} \circ \mathbf{T}_{\boldsymbol{\theta}^h} \,,\ \forall \bar{w} \in W^h_\mathbf{0} \right\} . \end{aligned}$$

Note that $V^h_{\boldsymbol{\theta}^h}$ ($W^h_{\boldsymbol{\theta}^h}$) is essentially the push-forward of $V^h_\mathbf{0}$ ($W^h_\mathbf{0}$) by $\mathbf{T}_{\boldsymbol{\theta}^h}$. We refer to Section 4.3 for more details on the finite-element structure in isogeometric analysis.

The discretization of (2) now reads:

$$\left.\begin{aligned} &\text{Find } (\boldsymbol{\theta}^h, u^h) \in \boldsymbol{\Theta}^h \times W^h_{\boldsymbol{\theta}^h} \text{ such that:} \\ &\quad \mathcal{B}((\boldsymbol{\theta}^h, u^h); v^h) = \mathcal{L}(\boldsymbol{\theta}^h; v^h) \qquad \forall v^h \in V^h_{\boldsymbol{\theta}^h} \,. \end{aligned}\right\} \tag{5}$$

0. Initialize: Choose a discrete displacement $\boldsymbol{\theta}_0^h \in \boldsymbol{\Theta}^h$; Set $k = 0$.
1. Given $\boldsymbol{\theta}_k^h$, solve the Neumann problem for u_k^h:

$$\left.\begin{array}{l} \text{Find } u_k^h \in V^h_{\boldsymbol{\theta}_k^h, u_{\mathcal{D}}} \text{ such that:} \\ \qquad \mathcal{B}((\boldsymbol{\theta}_k^h, u_k^h); v^h) = \mathcal{L}(\boldsymbol{\theta}_k^h; v^h) \qquad \forall v^h \in V^h_{\boldsymbol{\theta}_k^h} \,. \end{array}\right\}$$

2. Update the free-boundary displacement according to:

$$\tilde{\boldsymbol{\theta}}_{k+1}^h(\boldsymbol{\chi}) = \boldsymbol{\theta}_k^h(\boldsymbol{\chi}) + \alpha \frac{1 - u_k(\boldsymbol{x})}{g(\boldsymbol{x})} \boldsymbol{n}_k(\boldsymbol{x}) \,, \qquad \forall \boldsymbol{\chi} \in \Gamma_{\mathbf{0}} \,,$$

where $\boldsymbol{x} = \mathbf{T}_{\boldsymbol{\theta}_k^h}(\boldsymbol{\chi}) \in \Gamma_{\boldsymbol{\theta}_k^h}$, and subsequently project $\tilde{\boldsymbol{\theta}}_{k+1}^h$ onto $\boldsymbol{\Theta}^h$:

$$\boldsymbol{\theta}_{k+1}^h = \Pi_{\boldsymbol{\Theta}^h} \tilde{\boldsymbol{\theta}}_{k+1}^h \,.$$

3. Set $k \leftarrow k + 1$ and repeat from step 1. until convergence.

Figure 2: The explicit Neumann scheme for the solution of the discrete problem (5). In the first step, the solution space for u_k^h includes the Dirichlet condition *on* $\Gamma_{\mathcal{D}}$ *only* and is defined as $V^h_{\boldsymbol{\theta}_k^h, u_{\mathcal{D}}} \stackrel{\text{def}}{=} \{v = \bar{v} \circ \mathbf{T}_{\boldsymbol{\theta}_k^h} \,, \forall \bar{v} \in S^h \,|\, v = u_{\mathcal{D}} \text{ on } \Gamma_{\mathcal{D}}\}$. In the second step, $\boldsymbol{n}_k$ is the unit outward normal of $\Omega_{\boldsymbol{\theta}_k^h}$. Since $\tilde{\boldsymbol{\theta}}_{k+1}^h$ need not be in $\boldsymbol{\Theta}^h$, we need a projection operator $\Pi_{\boldsymbol{\Theta}^h}$ (e.g. L^2-projection) to obtain a new appropriate displacement $\boldsymbol{\theta}_{k+1}^h$. At this step one can also introduce relaxation to improve convergence. The parameter $\alpha \in [-1, 1]$ has to be chosen appropriately: $\alpha = 1$ corresponds to the *elliptic variant* and $\alpha = -1$ to the *hyperbolic variant*; see [18] for more details.

Remark 2.2 (Solution of (5)) The discrete problem (5) is highly nonlinear. To solve it, typically fixed-point-type algorithms are employed, also referred to as *trial free-boundary methods*. We have used a simple fixed-point algorithm referred to as the *explicit Neumann scheme* [18]. This scheme is outlined in Figure 2. The linearization techniques explained in Section 3 can also be used to derive Newton-type solution algorithms for (5). This is currently under investigation. □

3. Goal-oriented analysis of free-boundary problems

Goal-oriented error estimation starts with the identification of a quantity of interest, the so-called goal functional. Here, we consider the quantity introduced

in [35]:

$$Q(\boldsymbol{\theta}, u) \stackrel{\text{def}}{=} \int_{\Omega_{\boldsymbol{\theta}}} q^{\text{ave}}\, u \, \mathrm{d}x + \int_{\Gamma_{\mathbf{0}}} q^{\text{elev}}\, \alpha_{\boldsymbol{\theta}} \, \mathrm{d}s_{\mathbf{0}} \,,$$

where the weights q^{ave} and q^{elev} are assumed to be given, sufficiently smooth, functions. The first part in Q represents an interest in a weighted average of u. The second part in Q represents a (weighted) interest in the elevation $\alpha_{\boldsymbol{\theta}}(\boldsymbol{\chi})$ of the free boundary with respect to the reference configuration.

The key ingredient in the derivation of a goal-oriented error estimate is the dual problem. The dual problem is essentially a problem for the adjoint of the linearization of the primal problem (2), shortly referred to as the linearized-adjoint of (2). Driven by the quantity of interest, the solution to this dual problem indicates the precise influence of the residual on the error in Q. We shall make this statement precise in the following subsections, but we refer to the mentioned references in the introduction for more details on the general framework.

3.1. Three-step strategy to the linearized-adjoint problem

The linearized-adjoint of (2) has been derived in [36]. Let us provide a concise derivation of that result. The derivation is essentially based on the following three steps:

I. Derivation of a very-weak formulation;

II. Linearization of geometric nonlinearities using Hadamard formulas;

III. Interpretation of the linearized-adjoint problem.

Remark 3.1 (On linearizing free-boundary problems) For a *boundary-value problem*, the derivation of the linearized-adjoint simply amounts to the linearization of the weak form. For free-boundary problems, however, this is not adequate. The reason is that such a linearization does not take into account the Dirichlet condition $u = u_{\mathcal{D}}$ which holds on the unknown free boundary $\Gamma_{\boldsymbol{\theta}}$ and was incorporated into $W_{\boldsymbol{\theta}}$. The motivation for step I. is that a so-called very-weak formulation of the free-boundary problem *does* include the Dirichlet condition into the weak form. Compare this with the classical method using asymptotic expansions [7, 18]. □

Remark 3.2 (Domain-map linearization) Another approach to derive the linearized adjoint is presented in [35]. The main idea is to map the free-boundary problem to a fixed reference domain and then linearize with respect to the domain

map. The resulting linearized problem, however, contains impractical terms from an implementation point of view. In the context of fluid–structure interaction, this linearization technique can be found in [5, 17, 34]. The current three-step strategy applied to the linearized-adjoint of a fluid–structure interaction problem is presented in [33]. □

I. Derivation of a very-weak formulation. In the first step of the derivation, we perform an integration by parts of $\mathcal{B}((\boldsymbol{\theta}, u); v)$ (recall (3a)) and incorporate the Dirichlet boundary condition to arrive at the so-called very-weak formulation:

$$\mathcal{N}((\boldsymbol{\theta}, u); v) \overset{\text{def}}{=} -\int_{\Omega_{\boldsymbol{\theta}}} \left(u\,\Delta v + f\,v\right) \mathrm{d}x + \int_{\Gamma_{\boldsymbol{\theta}}} \left(-g\,v + u_{\mathcal{D}}\,\frac{\partial v}{\partial n}\right) \mathrm{d}s = 0$$

for all sufficiently smooth $v \in V_{\boldsymbol{\theta}}$.

II. Linearization of geometric nonlinearities using Hadamard formulas. In the second step, we linearize $\mathcal{N}((\boldsymbol{\theta}, u); v)$ and $\mathcal{Q}(\boldsymbol{\theta}, u)$ with respect to $(\boldsymbol{\theta}, u)$. These linearizations correspond to Gâteaux derivatives at a particular approximation $(\boldsymbol{\theta}^h, u^h)$ (not necessarily the Galerkin approximation (5)) in a direction $(\delta\boldsymbol{\theta}, \delta u)$. The key observation is that the linearization of the terms with respect to $\boldsymbol{\theta}$ are essentially shape derivatives. Therefore, such linearizations can be carried out using so-called Hadamard formulas [13, Ch. 8]. We summarize the result in the following theorem, the proof of which can be found in [36]. Notice that a curvature-dependent term $(-\kappa g v\,\delta\boldsymbol{\theta}\cdot\boldsymbol{n})$ appears through linearization.

Theorem 3.A (Linearization of $\mathcal{N}$ and $\mathcal{Q}$) *Given any approximation $(\boldsymbol{\theta}^h, u^h) \in \boldsymbol{\Theta}\times W_{\boldsymbol{\theta}^h}$, with $\boldsymbol{\theta}^h$ C^1-continuous (such that the discrete free-boundary $\Gamma_{\boldsymbol{\theta}^h}$ is also C^1-continuous).*[2] *Then, denoting by κ the curvature of the discrete free boundary $\Gamma_{\boldsymbol{\theta}^h}$, the Gâteaux derivative of $\mathcal{N}$ and $\mathcal{Q}$ is given by*[3]

$$\begin{aligned}
&\mathcal{N}'((\boldsymbol{\theta}^h, u^h); v)(\delta\boldsymbol{\theta}, \delta u) \\
&\qquad = \int_{\Omega_{\boldsymbol{\theta}^h}} -\delta u\,\Delta v \,\mathrm{d}x - \int_{\Gamma_{\boldsymbol{\theta}^h}} \left(g\,\frac{\partial v}{\partial n} + \left(f + \frac{\partial g}{\partial n} + \kappa\, g\right) v\right) \delta\boldsymbol{\theta}\cdot\boldsymbol{n}\,\mathrm{d}s\,, \\
&\mathcal{Q}'(\boldsymbol{\theta}^h, u^h)(\delta\boldsymbol{\theta}, \delta u) = \int_{\Omega_{\boldsymbol{\theta}^h}} q^{\text{ave}}\,\delta u\,\mathrm{d}x + \int_{\Gamma_{\boldsymbol{\theta}^h}} (q^{\text{ave}} + q^{\text{elev}})\,\delta\boldsymbol{\theta}\cdot\boldsymbol{n}\,\mathrm{d}s\,,
\end{aligned}$$

[2] To be precise, $\boldsymbol{\theta}^h$ should be $C^{1,1}$-continuous, where $C^{1,1}$ indicates Hölder-continuity of degree $(1, 1)$. This implies that the second derivative of $\boldsymbol{\theta}^h$, and thus the curvature, is bounded.

[3] The displacement perturbations $\delta\boldsymbol{\theta}$ are defined on the reference free boundary $\Gamma_{\boldsymbol{0}}$. Hence, in the formulas, they should be pulled back from $\Gamma_{\boldsymbol{\theta}^h}$ to $\Gamma_{\boldsymbol{0}}$, i.e. $\boldsymbol{x} \mapsto \delta\boldsymbol{\theta}(\boldsymbol{\chi}(\boldsymbol{x}))$.

for all $(\delta\boldsymbol{\theta}, \delta u) \in \boldsymbol{\Theta} \times V_{\boldsymbol{\theta}^h}$.

III. Interpretation of the linearized-adjoint problem. In the third step, we interpret the dual problem that is implied by the linearized-adjoint equation for the unknown dual variable $z \in V_{\boldsymbol{\theta}^h}$:

$$\mathcal{N}'((\boldsymbol{\theta}^h, u^h); z)(\delta u, \delta\boldsymbol{\theta}) = \mathcal{Q}'(\boldsymbol{\theta}^h, u^h)(\delta\boldsymbol{\theta}, \delta u) \;, \qquad \forall (\delta\boldsymbol{\theta}, \delta u) \in \boldsymbol{\Theta} \times V_{\boldsymbol{\theta}^h} \;. \tag{6}$$

It can easily be verified that the dual problem corresponds to the following boundary value problem on the approximate domain $\Omega_{\boldsymbol{\theta}^h}$:

$$-\Delta z = q^{\text{ave}} \qquad \text{in } \Omega_{\boldsymbol{\theta}^h} \;, \tag{7a}$$

$$g\frac{\partial z}{\partial n} + \Big(f + \frac{\partial g}{\partial n} + \kappa\, g\Big) z = -(q^{\text{ave}} + q^{\text{elev}}) \qquad \text{on } \Gamma_{\boldsymbol{\theta}^h} \;, \tag{7b}$$

$$z = 0 \qquad \text{on } \Gamma_{\mathcal{D}} \;. \tag{7c}$$

This is a Laplace problem with a curvature-dependent Robin boundary condition. We note again that the curvature term is bounded because of our continuity assumptions on the discrete free-boundary.

Remark 3.3 (Discretization of the dual problem) In goal-oriented error estimation of boundary-value problems, the linearized-adjoint equation in the form of (6) is often immediately suitable for finite-element discretizations. Here we see that (6) is not the natural weak formulation for a finite-element discretization of (7).[4] To discretize the dual problem, we therefore introduce the following separate weak formulation which imposes the Robin boundary condition in a weak manner:

$$\left.\begin{aligned} &\text{Find } z \in V_{\boldsymbol{\theta}^h} \text{ such that:} \\ &\int_{\Omega^h} \nabla z \cdot \nabla v \,\mathrm{d}x + \int_{\Gamma^h} \frac{f + \partial g/\partial n + \kappa\, g}{g}\, z\, v \,\mathrm{d}s \\ &\qquad = \int_{\Omega^h} q^{\text{ave}}\, v \,\mathrm{d}x + \int_{\Gamma^h} \frac{q^{\text{ave}} + q^{\text{elev}}}{g}\, v \,\mathrm{d}s \qquad \forall v \in V_{\boldsymbol{\theta}^h} \;. \end{aligned}\right\} \tag{8}$$

□

[4] This is also not necessary. All that is required is a suitable weak formulation for $z \in V_{\boldsymbol{\theta}^h}$ which is consistent with (6).

3.2. Goal-oriented error estimate

The main purpose of the so-derived dual problem is to provide an estimate for errors in the quantity of interest. Indeed, it can be shown that the following error representation holds; see [36] for a proof.

Theorem 3.B (Error representation) *Let $(\boldsymbol{\theta}, u)$ denote the solution to (2) and z the solution to the dual problem (8). Under the assumptions of Theorem 3.A, we have*

$$\mathcal{E}_Q \equiv Q(\boldsymbol{\theta}, u) - Q(\boldsymbol{\theta}^h, u^h) = \mathcal{R}((\boldsymbol{\theta}^h, u^h); z) + h.o.t.,$$

where the residual is

$$\mathcal{R}((\boldsymbol{\theta}^h, u^h); z) = \mathcal{L}(z) - \mathcal{B}((\boldsymbol{\theta}^h, u^h); z) \, .$$

To obtain a computable estimate of the error in Q, we need to compute an approximation z^{h_2} to the dual.[5] Neglecting the error in z and higher-order terms, we then obtain the estimate

$$\mathcal{E}_Q \equiv Q(\boldsymbol{\theta}, u) - Q(\boldsymbol{\theta}^h, u^h) \approx \mathrm{Est}(\boldsymbol{\theta}^h, u^h; z^{h_2}) \stackrel{\mathrm{def}}{=} \mathcal{R}((\boldsymbol{\theta}^h, u^h); z^{h_2}) \, . \tag{9}$$

4. Isogeometric shape functions

In isogeometric analysis, spline basis functions are used for the parameterization of the geometry as well as for the discretization of the field variables. The parameterization of the physical domain Ω^h and its boundaries, as introduced in Section 2.3, is established from a parameter domain $\hat{\Omega}$ via the reference domain $\Omega_{\mathbf{0}}$ by the composition $\mathbf{T}^h \circ \mathbf{F}^h$, where $\mathbf{F}^h$ maps $\hat{\Omega}$ onto $\Omega_{\mathbf{0}}$. We thus obtain from (4):

$$\boldsymbol{x} = \mathbf{T}^h(\boldsymbol{\chi}) = \mathbf{T}^h(\mathbf{F}^h(\boldsymbol{\xi})) = \sum_{i=1}^{n} \bar{N}_i(\mathbf{F}^h(\boldsymbol{\xi})) \, \boldsymbol{X}_i = \sum_{i=1}^{n} N_{i,p}(\boldsymbol{\xi}) \, \boldsymbol{X}_i \qquad \forall \boldsymbol{\xi} \in \hat{\Omega} \, ,$$

with control points $\{\boldsymbol{X}_i \in \mathbb{R}^2\}_{i=1}^n$ and $\bar{N}_i \circ \mathbf{F}^h = N_{i,p}$. Note that in this section, we explicitly denote the polynomial order of the n spline basis functions $\{N_{i,p}\}_{i=1}^n$ in the parameter domain using the subscript "p". Similarly, the free boundary

[5] Typically, the mesh used to compute the dual solution z^{h_2} is finer than the one used to compute u^h. This avoids Galerkin orthogonality rendering a useless estimate [3].

$\Gamma^h \ni \boldsymbol{x} = \mathbf{T}^h(\mathbf{F}^h(\boldsymbol{\xi}))$ is parameterized by the coordinate $\boldsymbol{\xi} \in \hat{\Gamma}$. This allows for the evaluation of the (bounded) curvature

$$\kappa = \frac{\left|\frac{\partial \boldsymbol{x}}{\partial \boldsymbol{\xi}} \times \frac{\partial^2 \boldsymbol{x}}{\partial \boldsymbol{\xi}^2}\right|}{\left|\frac{\partial \boldsymbol{x}}{\partial \boldsymbol{\xi}}\right|^3} \tag{10}$$

as required for solving the dual problem (7).

Since the same basis functions are used to discretize the primal and dual field variables, u and z, we have

$$u^h(\boldsymbol{x}) = \sum_{i=1}^{n} N_{i,p}(\boldsymbol{\xi}(\boldsymbol{x}))\, U_i \qquad \forall \boldsymbol{x} \in \Omega^h \ ,$$

$$z^h(\boldsymbol{x}) = \sum_{i=1}^{n} N_{i,p}(\boldsymbol{\xi}(\boldsymbol{x}))\, Z_i \qquad \forall \boldsymbol{x} \in \Omega^h \ ,$$

with control variables $\{U_i\}_{i=1}^n$ and $\{Z_i\}_{i=1}^n$. The basis functions can be constructed such that: i) the geometry can be respresented adequately; ii) the basis is appropriate for the problem under consideration. In particular this implies that the basis functions should be smooth along the free boundary Γ^h, while at other points on the boundary, locally reduced continuity can be required to represent kinks.

We first illustrate the most important properties of the employed spline technology for the fundamental building block of isogeometric analysis: the univariate B-spline. After that we introduce bivariate spline technologies that, for the problems discussed in this work, satisfy the two requirements mentioned above. We conclude this section with the introduction of a spline element technology, which facilitates the decoupling of the geometry and the physical problem.

4.1. The univariate B-spline basis

In the univariate case, the parameter domain $\hat{\Omega} = (\xi_1, \xi_k) \subset \mathbb{R}$ can be partitioned into $k-1$ subdomains of non-negative length by a knot vector $\Xi = \{\xi_1, \xi_2, \ldots, \xi_{k-1}, \xi_k\}$, with $\xi_1 \leq \xi_2 \leq \ldots \leq \xi_k$. A set of $n = k - p - 1$ piecewise constant basis functions, $\{N_{i,0}\}_{i=1}^{k-1}$, is provided by

$$N_{i,0}(\xi) = \begin{cases} 1 & \xi_i \leq \xi < \xi_{i+1} \ , \\ 0 & \text{otherwise.} \end{cases} \tag{11}$$

Sets of piecewise linear ($p = 1$) and higher-order ($p > 1$) basis functions, $\{N_{i,p}\}_{i=1}^{k-p-1}$, then follow using the Cox–de Boor [11, 12] recursion relation

$$N_{i,p}(\xi) = \frac{\xi - \xi_i}{\xi_{i+p} - \xi_i} N_{i,p-1}(\xi) + \frac{\xi_{i+p+1} - \xi}{\xi_{i+p+1} - \xi_{i+1}} N_{i+1,p-1}(\xi) \ . \tag{12}$$

We restrict ourselves to B-spline bases defined over open knot vectors, for which the first and last knot values are repeated $p + 1$ times. Open knot vectors (in one dimension) make the basis functions interpolatory at the boundaries of the parameter domain, i.e. $N_{1,p}(\xi_1) = N_{n,p}(\xi_k) = 1$, which eases the imposition of boundary conditions. The B-spline basis functions (11) and (12) are non-negative, satisfy the partition of unity property, and are variation diminishing. See [9] for a detailed discussion on the properties of B-spline basis functions.

For a knot vector with distinct knot values other than the first and last knot value, the B-spline basis functions of order p are $(p-1)$-times continuously differentiable, i.e. $N_{i,p} \in C^{p-1}(\hat{\Omega})$. For piecewise constant basis functions ($p = 0$) the basis functions are obviously discontinuous, while for piecewise linear basis functions ($p = 1$) continuous (but not continuously differentiable) basis functions are obtained. As outlined before, (at least) continuously differentiable basis functions are required in order to directly discretize the curvature-dependent Robin boundary condition eminating in the adjoint problem (8). By virtue of the definition of the B-spline basis functions, this continuity condition is naturally obtained using B-spline basis functions of order two or higher ($p \geq 2$). Since isogeometric analysis embodies the isoparametric paradigm, a local reduction of basis function continuity can be dictated by geometry requirements. For example, a kink in the geometry requires C^0-continuity of the basis functions at the position of that kink. The local continuity of the basis functions can be controlled by the multiplicity of knot values. For example, for a second-order B-spline basis function local C^0-continuity is obtained by creating a knot with multiplicity two at the position of the kink.

In computer aided geometric design (CAGD) use is often made of non-uniform rational B-splines (NURBS), because of their ability to exactly parameterize conic sections. The corresponding rational basis functions are obtained by the provision of a control point weight to every control point, from which a spline weighting function can be derived. See [9] for a detailed discussion on the use of NURBS in isogeometric analysis.

4.2. Spline patches and T-splines

A higher-order continuous B-spline basis can also be constructed over a multi-dimensional parameter domain $\hat{\Omega} = \hat{\Omega}^1 \otimes \ldots \otimes \hat{\Omega}^{n_v} \subset \mathbb{R}^{n_v}$, with n_v the dimension, and $\{\hat{\Omega}^i\}_{i=1}^{n_v}$ the univariate parameter domains as discussed above. The basis functions over this tensor-product domain are constructed by the provision of n_v (open)

knot vectors, $\Xi = \{\Xi^i\}_{i=1}^{n_v}$, to yield

$$N_{i,p}(\boldsymbol{\xi}) = \prod_{\alpha=1}^{n_v} N_{i,p}^{\alpha}(\boldsymbol{\xi}^i) \qquad \forall \boldsymbol{\xi} = (\xi^1, \ldots, \xi^{n_v}) \in \hat{\Omega} \,. \tag{13}$$

Bivariate ($n_v = 2$) B-spline bases are extensively used in CAGD for the parameterization of surfaces by means of a set of control points in two or three dimensions. We refer to these spline surfaces as B-spline patches. As in the univariate case, commonly a NURBS basis is used instead of a B-spline basis, because of its ability to exactly represent a broader range of geometric entities. For such a NURBS patch, the control points are supplemented with control point weights.

Although the types of domains that can be parameterized by a single tensor-product patch is fairly limited, combinations of tensor-product patches can be used for the parameterization of many geometric objects of engineering interest. In fact, bivariate NURBS patches are the industry standard in CAGD [29]. A detailed discussion on the combination of multiple NURBS patches in isogeometric analysis can be found in [9].

An alternative approach to handling complex geometric designs is provided by T-splines. In recent years T-splines have gained popularity in CAGD, and, more recently, in isogeometric analysis. T-splines abandon the concept of a global parameter domain. Instead, a local parameter domain is constructed for every T-spline basis function. As a consequence, local refinements can be constructed in a straightforward way and continuity conditions can be changed locally. These properties generally result in more efficient parameterizations in CAGD [31], and have proven to be useful in isogeometric analyses [4] in general, as well as in adaptive mesh-refinement strategies [15].

4.3. Bézier extraction

Exploiting the continuity properties of B-spline and T-spline basis functions, suitable bases can be created for the analysis of our free boundary problem (2). From an implementation point of view, an element representation of the globally defined spline objects is desirable, since all basis functions can then be constructed from a canonical set of basis functions defined over a parent element. Besides that, from an analysis point of view, such an element representation can provide a unified approach to B-spline patches, NURBS patches and T-splines. Bézier extraction has been proposed to obtain an element representation for B-splines, NURBS [6] and T-splines [30].

Bézier extraction defines elements as subdomains Ω_e of the physical domain Ω^h over which the basis functions are infinitely smooth, i.e. $N_i|_{\Omega_e} \in C^\infty(\Omega_e)$. Only subdomains with positive area are counted as elements. In the univariate setting this definition clearly identifies the elements as the knot intervals of positive length. For tensor-product patches the tensorial grid created by the knot vectors provides mesh lines similar to those encounterd in traditional finite elements. For a detailed discussion on the definition of elements in T-splines, see [30].

The restrictions of the B-spline or T-spline basis functions to an element, span the space of polynomials of order p over that element. As a consequence, the restricted basis functions can be represented as linear combinations of any set of basis functions spanning the same space. In Bézier extraction we define the Bernstein basis $\{B_{i,p}\}_{i=1}^{(p+1)^{n_v}}$, see [30], over a parent element as the canonical set of polynomials from which all basis functions are constructed. The restricted, globally smooth, basis functions can then be expressed in terms of the Bernstein basis as

$$N_{i,p}(\boldsymbol{\xi})|_{\Omega_e} = \tilde{N}_{i,p}(\tilde{\boldsymbol{\xi}}) = C^e_{ij} B_{j,p}(\tilde{\boldsymbol{\xi}}) \tag{14}$$

which requires the provision of a map between the parent element domain $\tilde{\Omega}$ and the physical element domain Ω_e. We refer to the matrix C^e as the element extraction operator. The isoparametric parent element supplemented with an extraction operator is called a Bézier element. Efficient algorithms for deriving the element extraction operators for NURBS patches and T-splines are provided in [6] and [30], respectively. We illustrate the Bézier extraction concept for the B-spline case in Figure 3.

For analysis purposes all topology and continuity information can be stored in a Bézier mesh, which consists of:

- A collection of Bézier elements over which the set of canonical basis functions is defined. As in traditional finite element meshes, for every element, the `IEN`-array [21] provides the list of indices of nonzero basis functions over that element. In addition the element extraction operator C^e provides the map from the canonical set of basis functions to the globally smooth basis functions.

- A global set of control points, possibly supplemented with control weights, commonly referred to as the control net.

Note that the number of rows in the element extraction operator is equal to the number of nonzero global basis functions supported by an element. The number

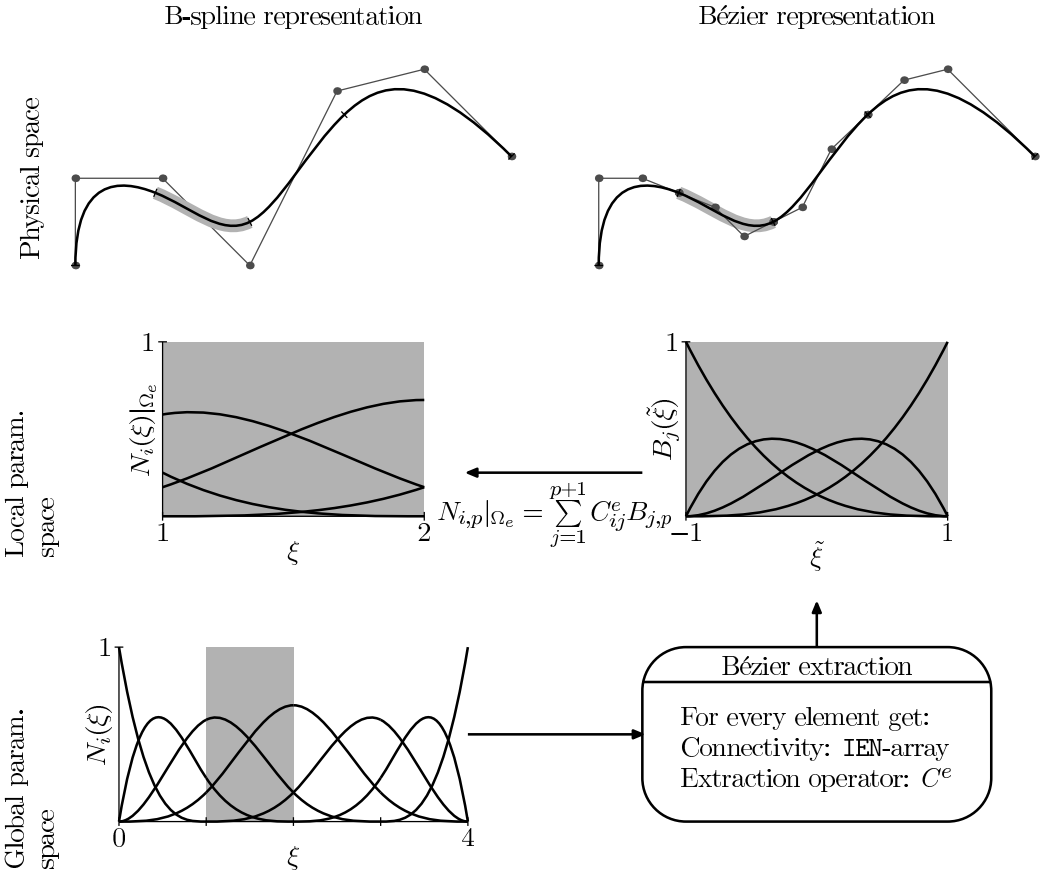

Figure 3: Schematic representation of Bézier extraction for a third-order ($p = 3$) B-spline constructed from the open knot vector $\Xi = \{0, 0, 0, 0, 1, 2, 3, 4, 4, 4, 4\}$. The global basis functions over element number 2, i.e. $\Omega_2 = (1, 2)$, are expressed in terms of the Bernstein basis over the parent element domain.

of columns is equal to the number of Bernstein shape functions defined over the parent element. The number of canonical basis functions is equal to $(p + 1)^{n_v}$, whereas the number of supported global basis functions can differ from this. Consequently, the extraction operator is in general not a square matrix.

For the problems considered in this work the Bézier meshes consist of both bivariate and univariate Bézier elements. The former are used for the discretization of the interior of the domain, whereas the latter are used for the discretization of the free boundary. As in traditional finite elements, the connectivity information for the boundary elements can be obtained from the internal elements. The same is true for the boundary element extraction operators.

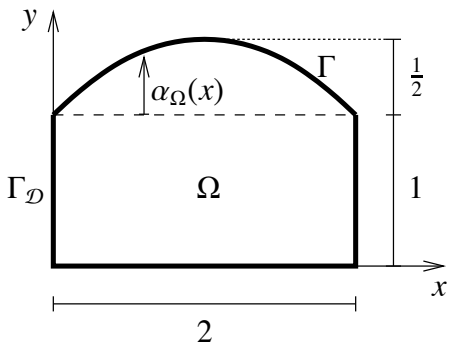

Figure 4: Problem set-up for the parabolic-free-boundary test case.

5. Numerical simulations

We consider two test cases [36] to illustrate the suitability of isogeometric finite elements for the discretization of the Bernoulli free-boundary problem and its linearized adjoint. We furthermore present the corresponding dual-based error-estimates (Est($\boldsymbol{\theta}^h, u^h; z^{h_2}$) in (9)). In the first case we consider a rectangular domain (in its undeformed configuration), for which a suitable mesh is obtained using a single B-spline patch. For the second numerical simulation we consider a domain with a notch, which requires the construction of a T-spline-based discretization.

5.1. Parabolic-free-boundary test case

We first investigate the dual-based error estimate for the free-boundary problem schematically shown in Figure 4. The Dirichlet boundary conditions are chosen as $u_\mathcal{D}|_{\Gamma_\mathcal{D}} = y$ and $u_\mathcal{D}|_{\Gamma^h} = 1$. The Neumann boundary condition g on the free boundary Γ and f on Ω are chosen such that the solution is a parabolic deformation of the free-boundary, i.e. $\alpha_\Omega(x) = \frac{1}{2}x(2-x)$, and

$$u(x,y) = \frac{y}{1+\alpha_\Omega(x)} + \alpha_\Omega(x)\frac{y}{1+\alpha_\Omega(x)}\left(1 - \frac{y}{1+\alpha_\Omega(x)}\right) . \tag{15}$$

Our interest pertains to the average goal with $q^{\text{ave}} = 1$, for which the value at the exact solution is $Q^{\text{ave}}(\Omega; u) = \frac{67}{45} = 1.4888\ldots$.

In Table 1 we list the results obtained on various meshes. A mesh convergence plot is shown in Figure 5. As can be seen, a significant increase in convergence rate is obtained when increasing the order of the B-spline discretization from one to two. Since the computation of the dual problem requires C^1-continuity, meaningful results cannot be obtained on the first-order meshes. Consequently, all

results discussed in the remainder of this section are obtained using second-order B-splines. It is important to note that the number of degrees of freedom in the case of B-splines is practically independent of the order of the splines. For example, on the 32×16-mesh, the number of first-order basis functions is equal to 561, whereas 612 second-order basis functions are present.

To compute the error estimates, the dual solutions are computed on meshes which are two times uniformly refined. For example, the error estimate for the 4×2 elements mesh is computed using the dual solution on the 16×8 mesh. Typical solutions of the primal and dual problem are shown in Figure 6. The resulting error estimates are presented in Table 1. We have also computed the effectivity which is defined as the estimate divided by the true error. It is observed that upon refinement of the mesh, the effectivity index approaches one. This illustrates the higher-order consistency of the dual-based estimate with respect to the true error. As the mesh is refined, the linearization error in the estimate goes quicker to zero than the error itself.

Table 1: Results for the parabolic-free-boundary test case. The goal average is equal to $Q^{\text{ave}} = \frac{67}{45} = 1.488888\ldots$ at the exact solution.

Elements	Dofs	Q^{ave}	$\mathcal{E}_{Q^{\text{ave}}}$	$\text{Est}_{Q^{\text{ave}}}$	Effectivity
2	12	1.488376	$5.126 \cdot 10^{-4}$	$1.405 \cdot 10^{-3}$	2.740
8	24	1.492078	$-3.189 \cdot 10^{-3}$	$-3.078 \cdot 10^{-3}$	0.965
32	60	1.489346	$-4.569 \cdot 10^{-4}$	$-4.475 \cdot 10^{-4}$	0.980
128	180	1.488956	$-6.725 \cdot 10^{-5}$	$-6.688 \cdot 10^{-5}$	0.995
512	612	1.488898	$-9.352 \cdot 10^{-6}$	$-9.352 \cdot 10^{-6}$	1.000
2048	2244	1.488890	$-1.330 \cdot 10^{-6}$	-	-
8192	8580	1.488889	$-1.963 \cdot 10^{-7}$	-	-
∞	∞	1.488888	0	-	-

5.2. Notched channel test case

In the second test case, we consider the notched channel shown in Figure 7. The Dirichlet boundary condition $u_{\mathcal{D}}|_{\Gamma_{\mathcal{D}}}$ is equal to zero on the bottom of the domain and equal to the y-coordinate along the left and right side of the domain. On the free boundary Γ^h, $u_{\mathcal{D}} = 1$ and $g = 0$. Moreover, f is equal to zero over the interior of the domain. Our goal quantity is the elevation of the free boundary $\alpha_\theta(x)$ at $x = 2 + \sqrt{2}$. Note that this point-wise quantity of interest corresponds to a nonsmooth q^{elev} (of Dirac delta-type).

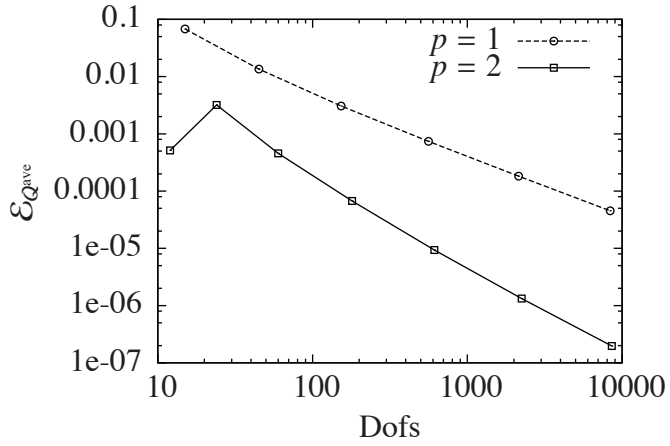

Figure 5: Dependence of the error in the goal functional Q^{ave} on the number of degrees of freedom for uniformly refined meshes.

From a numerical modeling point of view, this problem set-up poses various challenges. On the one hand, a direct discretization of the dual problem boundary conditions requires the free boundary to be continuously differentiable. On the other hand, the kinks in the bottom of the domain require local C^0-continuity. Since in isogeometric analysis the same basis is used for the parameterization of the geometry and the discretization of the field variables, both these features need to be embedded in the spline basis. This cannot be established with a single B-spline patch, since in that case the reduction in local continuity at the bottom of the domain (which would be created by local knot insertion) would propagate to the top boundary, causing a singular free boundary curvature. The simultaneous satisfaction of both continuity requirements can, however, be established by a third order T-spline. The control net for the employed T-spline is shown in Figure 8, both in the undeformed and deformed configuration. The insertion of additional zero knot intervals around the kinks in te bottom boundary is reflected by the presence of additional control points around those kinks. The basis functions associated with the control points around the kinks are not continuously differentiable. Since these basis functions stretch out two elements in the domain, they do not reach the top boundary. Consequently, all non-zero basis function on the top boundary are still continuously differentiable, and all continuity requirements for the problem under consideration are satisfied.

Besides the T-spline control net in Figure 8 we show the resulting Bézier elements. The solution of the Bernoulli problem has been computed on five succesive

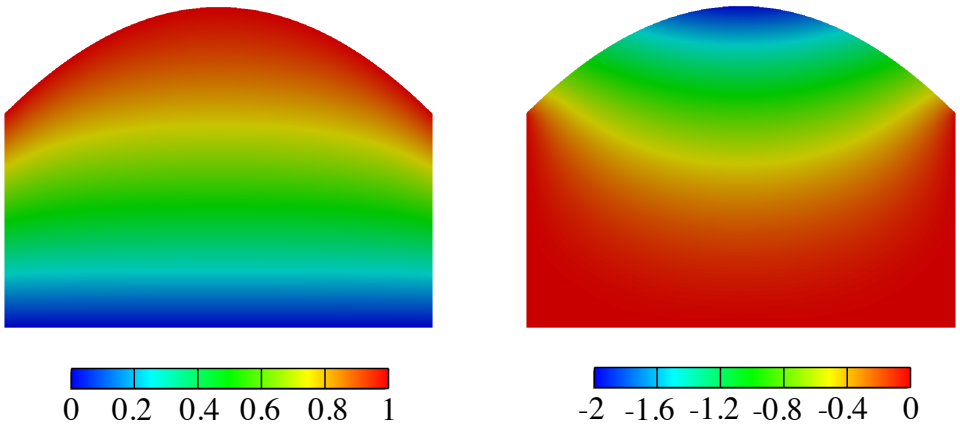

Figure 6: Contour plots showing (left) the primal solution and (right) the dual solution for the parabolic test case.

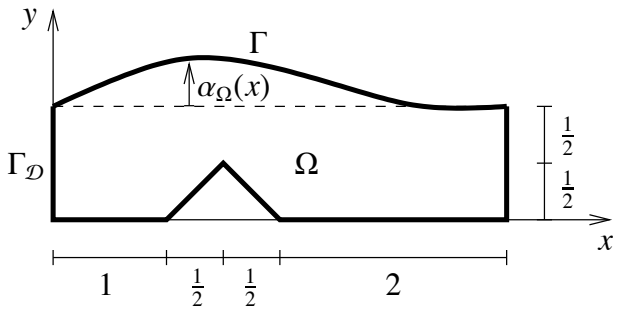

Figure 7: Problem set-up for the notched channel free-boundary test case.

uniform refinements of this mesh. The first two refinements, consisting of 64 and 256 elements, are shown in Figure 9. The results are presented in Table 2, and a mesh convergence curve is shown in Figure 10. As can be seen, the convergence rate is not optimal due to the presence of singularities in the primal and dual solution. The dual solution used to compute the error-estimate is obtained on a two-times refined mesh. Typical solutions for the primal and dual problem are shown in Figure 11. The fact that the effectivity converges to a value different from one means that the error in the estimate is of the same order as the error itself. It is believed that this error in the estimate comes from the fact that the dual solution, visible in Fig. 11 (right), is singular. Therefore, the computed dual approximations have a slow convergence limiting the accuracy of the estimate (with a constant factor though).

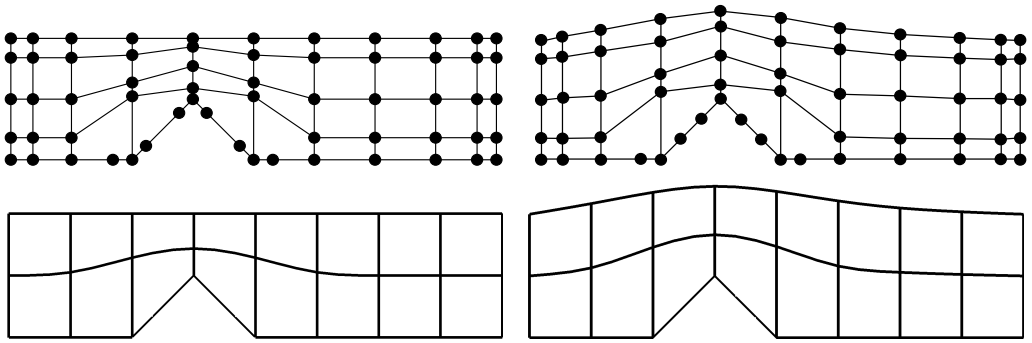

Figure 8: Control net (top row) and Bézier elements (bottom row) for the coarsest mesh used to discretize the notched channel problem in the undeformed (left column) and deformed configuration (right column).

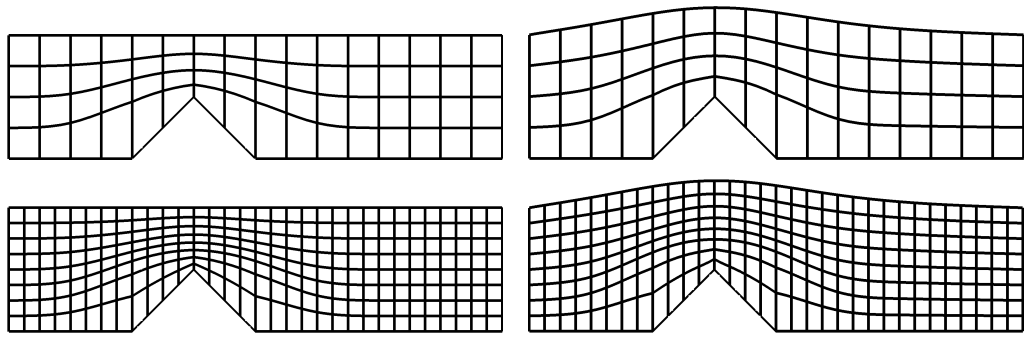

Figure 9: Two succesive uniform refinements of the coarsest Bézier mesh in undeformed (left column) and deformed configuration (right column). The top row meshes consist of 4×16 Bézier elements. The bottom row meshes have 8×32 elements.

6. Concluding remarks

The linearization with respect to geometry is as old as calculus itself. Indeed, in the one-dimensional setting, differentiation under the integral sign can be done using the Leibniz integral rule. Modern origins of shape calculus are attributed to various mathematicians in French Schools of Applied Mathematics [20, 27, 38]. Historically, (linearized-) adjoints have been of prime importance in the fields of optimal control and shape optimization. Meanwhile, adjoints in goal-oriented analysis are becoming more and more prominent, finding various new applications [26].

In the context of free-boundary problems, and interface problems in general (such as fluid–structure interaction), a major bottleneck in the implementation

Table 2: Results for the notched channel free-boundary problem. The reference solution for the goal quantity is taken as $Q^{\text{elev}} = 0.02269$.

Elements	Dofs	Q^{elev}	$\mathcal{E}_{Q^{\text{elev}}}$	$\text{Est}_{Q^{\text{elev}}}$	Effectivity
16	61	0.02372	$-1.03 \cdot 10^{-3}$	$-5.01 \cdot 10^{-4}$	0.49
64	145	0.02292	$-2.31 \cdot 10^{-4}$	$-8.16 \cdot 10^{-5}$	0.35
256	409	0.02279	$-9.52 \cdot 10^{-5}$	$-3.39 \cdot 10^{-5}$	0.36
1024	1321	0.02273	$-4.33 \cdot 10^{-5}$	$-1.55 \cdot 10^{-5}$	0.36
4096	4681	0.02271	$-8.09 \cdot 10^{-6}$	-	-
16384	17545	0.02270	-	-	-

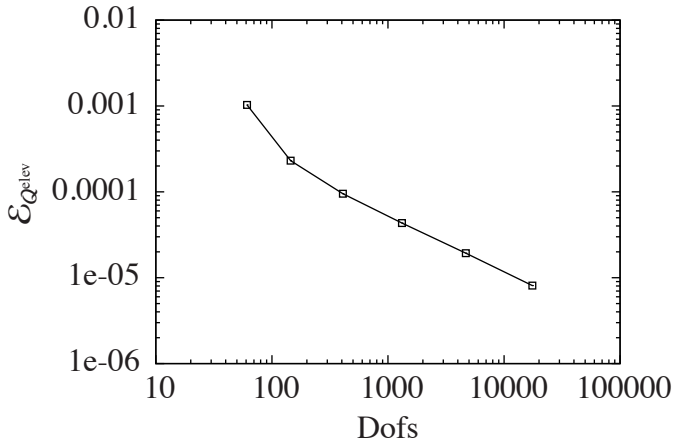

Figure 10: Dependence of the error in the goal functional on the number of degrees of freedom.

of the adjoint is the required smoothness of the discrete boundaries (and also the smoothness of the field variables defined there, in general). Example adjoint boundary conditions in the case of fluid–structure interaction can be found in [25, Eq. (8.12)] and [33]. The example studied in this work, although elementary, shows that isogeometric finite elements provide, in a practical and unifying manner, the realization of such adjoints.

Acknowledgement

The first author's work on this paper was completed while he was a Postdoctoral Fellow at the Institute for Computational Engineering and Sciences at The University of Texas at Austin under support of the DOE Multiscale Mathematics Contract DE-FG02-05ER25701.

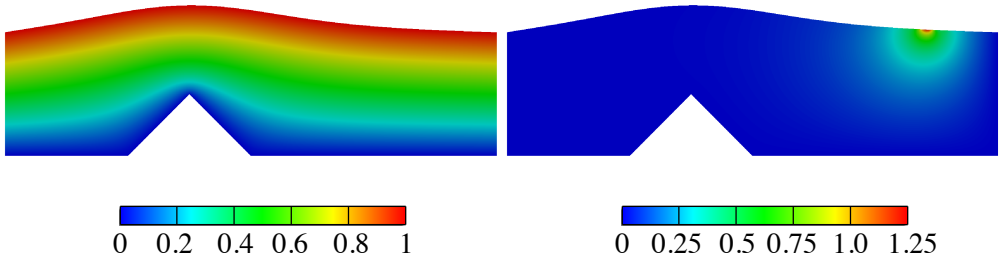

Figure 11: Contour plots showing (left) the primal solution and (right) the dual solution for the notched channel problem.

References

[1] M. Ainsworth and J. T. Oden, *A Posteriori Error Estimation In Finite Element Analysis*, Pure Appl. Math., Wiley, 2000.

[2] I. Akkerman, Y. Bazilevs, V. M. Calo, T. J. R. Hughes, and S. Hulshoff, *The role of continuity in residual-based variational multiscale modeling of turbulence*, Comput. Mech., 41 (2008), pp. 371–378.

[3] W. Bangerth and R. Rannacher, *Adaptive Finite Element Methods for Differential Equations*, Lectures in Mathematics, ETH Zürich, Birkhäuser, 2003.

[4] Y. Bazilevs, V. M. Calo, J. A. Cottrell, J. A. Evans, T. J. R. Hughes, S. Lipton, M. A. Scott, and T. W. Sederberg, *Isogeometric analysis using T-splines*, Comput. Methods Appl. Mech. Engrg., 199 (2010), pp. 229–263.

[5] Y. Bazilevs, V. M. Calo, T. J. R. Hughes, and Y. Zhang, *Isogeometric fluid–structure interaction: Theory, algorithms, and computations*, Comput. Mech., 43 (2008), pp. 3–37.

[6] M. J. Borden, M. A. Scott, J. A. Evans, and T. J. R. Hughes, *Isogeometric finite element data structures based on Bézier extraction*, Internat. J. Numer. Meth. Engrg., (2010). doi: 10.1002/nme.2968.

[7] F. Bouchon, S. Clain, and R. Touzani, *A perturbation method for the numerical solution of the Bernoulli problem*, J. Comput. Math., 26 (2008), pp. 23–36.

[8] A. Buffa, G. Sangalli, and R. Vázquez, *Isogeometric analysis in electromagnetics: B-splines approximation*, Comput. Methods Appl. Mech. Engrg., 199 (2010), pp. 1143–1152.

[9] J. A. Cottrell, T. J. R. Hughes, and Y. Bazilevs, *Isogeometric Analysis: Toward Integration of CAD and FEA*, John Wiley & Sons, Chichester, UK, 2009.

[10] J. A. Cottrell, A. Reali, Y. Bazilevs, and T. J. R. Hughes, *Isogeometric analysis of structural vibrations*, Comput. Methods Appl. Mech. Engrg., 195 (2006), pp. 5257–5296.

[11] M. G. Cox, *The numerical evaluation of B-splines*, IMA J. Appl. Math., 10 (1972), pp. 134–149.

[12] C. de Boor, *On calculating with B-splines*, J. Approx. Theory, 6 (1972), pp. 50–62.

[13] M. C. Delfour and J.-P. Zolésio, *Shapes and Geometries: Analysis, Differential Calculus, and Optimization*, vol. 4 of SIAM Series on Advances in Design and Control, Society for Industrial and Applied Mathematics, 2001.

[14] J. Donea, A. Huerta, J.-P. Ponthot, and A. Rodríguez-Ferran, *Arbitrary Lagrangian–Eulerian methods*, in Encyclopedia of Computational Mechanics, E. Stein, R. de Borst, and T. J. R. Hughes, eds., vol. 1: Fundamentals, John Wiley & Sons, 2004, ch. 14, pp. 413–437.

[15] M. R. Dörfel, B. Jüttler, and B. Simeon, *Adaptive isogeometric analysis by local h-refinement with T-splines*, Comput. Methods Appl. Mech. Engrg., 199 (2010), pp. 264–275.

[16] C. Farhat, *CFD-based nonlinear computational aeroelasticity*, in Encyclopedia of Computational Mechanics, E. Stein, R. de Borst, and T. J. R. Hughes, eds., vol. 3: Fluids, John Wiley & Sons, 2004, ch. 13, pp. 459–480.

[17] M. A. Fernández and M. Moubachir, *A Newton method using exact Jacobians for solving fluid–structure interaction*, Comput. & Structures, 83 (2005), pp. 127–142.

[18] M. Flucher and M. Rumpf, *Bernoulli's free-boundary problem, qualitative theory and numerical approximation*, J. Reine Angew. Math., 486 (1997), pp. 165–204.

[19] H. Gómez, V. M. Calo, Y. Bazilevs, and T. J. R. Hughes, *Isogeometric analysis of the Cahn–Hilliard phase-field model*, Comput. Methods Appl. Mech. Engrg., 197 (2008), pp. 4333–4352.

[20] J. S. Hadamard, *Mémoire sur le problème d'analyse relatif à l'équilibre des plaques élastiques encastrées*, in Œuvres de Jacques Hadamard, C.N.R.S. Editions, Paris, 1968, pp. 515–641. Originally published in Mém. Sav. Étrang., 33, 1907.

[21] T. J. R. Hughes, *The Finite Element Methods: Linear Static and Dynamic Finite Element Analysis*, Dover Publications, Mineola, New York, 2000.

[22] T. J. R. Hughes, J. A. Cottrell, and Y. Bazilevs, *Isogeometric analysis: CAD, finite elements, NURBS, exact geometry and mesh refinement*, Comput. Methods Appl. Mech. Engrg., 194 (2005), pp. 4135–4195.

[23] K. T. Kärkkäinen and T. Tiihonen, *Free surfaces: Shape sensitivity analysis and numerical methods*, Internat. J. Numer. Meth. Engrg., 44 (1999), pp. 1079–1098.

[24] N. P. Kruyt, C. Cuvelier, A. Segal, and J. van der Zanden, *A total linearization method for solving viscous free boundary flow problems by the finite element method*, Internat. J. Numer. Meth. Fluids, 8 (1988), pp. 351–363.

[25] M. Moubachir and J.-P. Zolésio, *Moving Shape Analysis and Control, Applications to Fluid Structure Interactions*, Pure and Applied Mathematics, Chapman & Hall/CRC, 2006.

[26] J. T. Oden, I. Babuška, F. Nobile, Y. Feng, and R. Tempone, *Theory and methodology for estimation and control of errors due to modeling, approximation, and uncertainty*, Comput. Methods Appl. Mech. Engrg., 194 (2005), pp. 195–204.

[27] O. Pironneau, *Optimal Shape Design for Elliptic Systems*, Springer Series in Computational Physics, Springer, Berlin, 1984.

[28] S. Prudhomme and J. T. Oden, *Computable error estimators and adaptive techniques for fluid flow problems*, in Error Estimation and Adaptive Discretization Methods in Computational Fluid Dynamics, T. J. Barth and H. Deconinck, eds., vol. 25 of Lecture Notes in Computational Science and Engineering, Springer-Verlag, Heidelberg, 2003, pp. 207–268.

[29] D. F. Rogers, *An Introduction to NURBS*, Academic Press, San Diego, 2001.

[30] M. A. Scott, M. J. Borden, C. V. Verhoosel, T. W. Sederberg, and T. J. R. Hughes, *Isogeometric finite element data structures based on Bézier extraction of T-splines*, tech. rep., Institute for Computational Engineering and Sciences (ICES), The University of Texas at Austin, Austin, Texas, 2010.

[31] T. W. Sederberg, J. Zheng, A. Bakenov, and A. Nasri, *T-splines and T-NURCCs*, ACM Trans. on Graphics, 22 (2003), pp. 477–484.

[32] J. Sokołowski and J.-P. Zolésio, *Introduction to Shape Optimization: Shape Sensitivity Analysis*, vol. 16 of Springer Series in Computational Mathematics, Springer-Verlag, 1992.

[33] K. G. van der Zee, E. H. van Brummelen, I. Akkerman, and R. de Borst, *Goal-oriented error estimation and adaptivity for fluid–structure interaction using exact linearized adjoints*, Comput. Methods Appl. Mech. Engrg., (submitted).

[34] K. G. van der Zee, E. H. van Brummelen, and R. de Borst, *Goal-oriented error estimation for Stokes flow interacting with a flexible channel*, Internat. J. Numer. Meth. Fluids, 56 (2008), pp. 1551–1557.

[35] ——, *Goal-oriented error estimation and adaptivity for free-boundary problems: The domain-map linearization approach*, SIAM J. Sci. Comput., 32 (2010), pp. 1064–1092.

[36] ——, *Goal-oriented error estimation and adaptivity for free-boundary problems: The shape linearization approach*, SIAM J. Sci. Comput., 32 (2010), pp. 1093–1118.

[37] C. V. Verhoosel, M. A. Scott, T. J. R. Hughes, and R. de Borst, *An isogeometric analysis approach to gradient damage models*, Tech. Rep. ICES 10-21, Institute for Computational Engineering and Sciences (ICES), The University of Texas at Austin, Austin, Texas, June 2010.

[38] J.-P. Zolésio, *Introduction to shape optimization problems and free boundary problems*, in Shape Optimization and Free Boundaries, M. C. Delfour and G. Sabidussi, eds., vol. 380 of NATO ASI Series C: Mathematical and Physical Sciences, Kluwer Academic Publishers, 1992, pp. 397–457.